Hyperfine Interact (2016) 237: 129
DOI 10.1007/s10751-016-1339-9

The influence of coordinated defects on inhomogeneous broadening in cubic lattices

P. L. Matheson[1] · **Francis P. Sullivan**[1] · **William E. Evenson**[1]

Published online: 23 August 2016

Abstract The joint probability distribution function (JPDF) of electric field gradient (EFG) tensor components in cubic materials is dominated by coordinated pairings of defects in shells near probe nuclei. The contributions from these inner shell combinations and their surrounding structures contain the essential physics that determine the PAC-relevant quantities derived from them. The JPDF can be used to predict the nature of inhomogeneous broadening (IHB) in perturbed angular correlation (PAC) experiments by modeling the G_2 spectrum and finding expectation values for V_{zz} and η. The ease with which this can be done depends upon the representation of the JPDF. Expanding on an earlier work by Czjzek et al. (Hyperfine Interact. **14**, 189–194, 1983), Evenson et al. (Hyperfine Interact. **237**, 119, 2016) provide a set of coordinates constructed from the EFG tensor invariants they named W_1 and W_2. Using this parameterization, the JPDF in cubic structures was constructed using a point charge model in which a single trapped defect (TD) is the nearest neighbor to a probe nucleus. Individual defects on nearby lattice sites pair with the TD to provide a locus of points in the $W_1 - W_2$ plane around which an amorphous-like distribution of probability density grows. Interestingly, however, marginal, separable PDFs appear adequate to model IHB relevant cases. We present cases from simulations in cubic materials illustrating the importance of these near-shell coordinations.

Keywords PAC · Inhomogeneous broadening

This article is part of the Topical Collection on *Proceedings of the International Conference on Hyperfine Interactions and their Applications (HYPERFINE 2016), Leuven, Belgium, 3–8 July 2016*

✉ P. L. Matheson
phil.matheson@uvu.edu

[1] Department of Physics, Utah Valley University, Orem, UT 84058, USA

1 Introduction

Since there no net electric field gradient (EFG) at sites of cubic symmetry, the hyperfine splitting of the nuclear spin state of a probe nucleus in such cases is caused by defects in the lattice. The EFG experienced by a probe nucleus is most strongly influenced by a single trapped defect (TD), arbitrarily chosen to be positively charged, in the first shell. When the influence of these nearest neighbor defects is the only contribution to the background EFG, the splitting is proportional to the EFG component V_{zz}. The EFG tensor is then axisymmetric and the components in arbitrary units are $V_{zz} = 2$, and $V_{xx} = V_{yy} = -1$ yielding an asymmetry parameter $\eta = \frac{2V_{xx}+V_{zz}}{V_{zz}} = 0$. This limiting case corresponds to a material with a very low concentration of defects. The resulting PAC G_2 spectrum contains three sharp peaks at frequencies, $\omega_1 = \frac{1}{2}\omega_2 = \frac{1}{3}\omega_3 = 6\omega_Q$, where ω_Q is the fundamental nuclear quadrupole frequency. With increasing defect concentrations, the EFG tensor contains ever more contributions from defects beyond the TD and the spectral peaks, ω_1, ω_2 and ω_3 are broadened and shifted. This phenomenon is called inhomogeneous broading (IHB). IHB also results in the time decay of G_2.

For polycrystalline materials considered here, the components of the diagonalized EFG tensor are fully characterized by two independent parameters or variables. For the most manageable representation, these should be statistically independent. In general, these cannot be V_{zz} and η as these show correlated behavior. However, were the joint probability distribution function (JPDF) of two suitable EFG coordinates known, then IHB and other PAC-relevant phenomena could be readily characterized by integration against the JPDF. For example if the two EFG coordinates were labeled W_1 and W_2, giving $P(W_1, W_2)$ as the JPDF, then the time-dependent PAC spectrum would be $G_2(t) = \int G_2(W_1, W_2, t)P(W_1, W_2)dW_1dW_2$, while the characteristic asymmetry parameter for the situation would simply be $< \eta >= \int \eta(W_1, W_2)P(W_1, W_2)dW_1dW_2$, etc. The JPDF can be found in principle from distributions of defects within a given lattice and the subsequent examination of EFG tensor components.

It is useful to contrast the possible JPDFs that may arise in cubic structures with the limiting case of materials that are isotropic, on average, containing a random distribution of defects. Czjzek et al. [3] determined the approximate limiting form for the JPDF for this situation in terms of V_{zz} and η by essentially summing over the Euler angles of the EFG components. The resulting analytic expression is a smoothly continuous bimodally-peaked function in V_{zz} and η. It is dependent on the EFG tensor invarients, $S = V_{zz}^2(1 + \eta^2/3)$, which aside from a constant multiplier is the sum of the squares of the individual EFG components and $D = V_{zz}^3(1 - \eta^2)$ which is simply four times the EFG tensor determinant. They found that non-zero values of D skewed the distribution making the density of positive and negative values of V_{zz} asymmetric about the origin. They attributed this distortion to the occupancy of the inner coordination shells and verified this with numerical simulations. The simulations showed that even a small number of defects in the inner coordination shells produced strong asymmetries. Whether the preponderance of V_{zz} probability density was positive or negative depended on whether these charged defects were tightly clustered near a single spot in the shell (or in two spots along an axis) or whether the charge distribution was more ring-like. The former case gave rise to more positive density, the latter to more negative. The two cases reflect whether the EFG distribution is respectively more prolate or oblate along a particular axis.

Similar results should be expected in cubic lattices with the following distinctions. The JPDF cannot be a smooth function. Each discrete configuration of charged defects maps to

a distinct point in the plane of EFG coordinates. The finite number of combinations in the inner shells which have the most influence do not fill the coordinate plane. This means that the JPDF will be "spiky" in the sense that if there are just a few restricted configurations of charges in the inner coordination shells, then these will produce discrete loci around which probability density will accumulate as these few configurations combine with the effects of more distant and more variable charge configurations. This produces a distribution of myriad peaks that never combine into a wholly smooth distribution. This is an effect of the EFG's inverse cube dependence on distance from the probe. It insures that the loci of points established by the coordinated pairs of inner shell defects never develop enough probability density about them to smoothly blend into other peaks.

For example, consider again the case at the beginning of this section. In any given cubic structure there is a TD near each of many probe nuclei but if the defect concentration is otherwise low enough, then the likelihood of finding a defect in another nearby coordination shell is negligible. The resulting JPDF should consist of a single sharp peak broadened only slightly by the contribution of remote defects [4]. The defects in distant shells are very nearly amorphous and the probability density they produce around the sharp peak would essentially follow that of Czjzek's analysis. The location of the peak essentially represents a shift in the origin of coordinates in the description of the JPDF due to an otherwise amorphous distribution of defects.

For a second example consider a cubic structure with one TD in shell 1 about a probe nucleus having a defect concentration high enough to also have a defect in shell 2. For the cubic lattices the combined EFG of the TD and the defect in shell 2 give rise to two possible points in any given EFG coordinate plane. The JPDF would then have two additional peaks corresponding to each of these sets. These peaks would be surrounded by numerous points corresponding to the many possible configurations of distant defects coupling with these two inner shell configurations. This immediately leads to a skewing of the JPDF and corresponds to the prolate or oblate skewing of the amorphous distributions discussed by Czjzek [3].

Evenson et al. [2, 5] examined which coordinate representation might best represent the JPDF of EFG components. Their study sought to find a separable JPDF that could be expressed as the product of two independent PDFs, one for each independent coordinate. Their investigations led them to conformally map the restricted 60° parameter space of Czjzek's [1, 3] coordinates to a half plane. In so doing they found that Czjzek's coordinates naturally map to the tensor invariants, S and D and they defined the coordinates as follows:

$$W_1 = \frac{8}{3\sqrt{3}}\eta(9-\eta^2)|V_{zz}|^3 = \sqrt{S^3 - D^2} \quad \text{and} \quad W_2 = 8(1-\eta^2)V_{zz}^3 = 8D \qquad (1)$$

These EFG coordinates have the advantage of smoothly using the half plane to cover the range of $0 \leq \eta \leq 1$ and all possible values of V_{zz}. Using the same arbitrary units as above, the limiting case of low defect concentration with one TD near each probe is $W_1 = 0$ and $W_2 = 64$. In this same limit W_1 is a proxy for η and W_2 for V_{zz}^3.

Using Evenson's parameterization, concentration-dependent JPDFs can be found from simulations. A random distribution of defects in a simulated crystal structure is mapped to a particular point in the W_1-W_2 plane. Repeating the procedure an arbitrarily large number of times allows the accumulation of the JPDF, $P(W_1, W_2, c)$, now a function of the defect concentration c. As discussed above, the JDPFs are unavoidably spiky and asymmetric. Nevertheless, with the ultimate aim of characterizing PAC features, approximately separable PDFs, $P(W_1, W_2, c) = P_1(W_1, c)P_2(W_2, c)$ are constructed with the implicit assumption

that W_1 and W_2 may be used as independent variables. This is done by using marginal distributions. That is

$$P_1(W_1, c) = \int P(W_1, W_2, c) dW_2 \text{ and } P_2(W_2, c) = \int P(W_1, W_2, c) dW_1. \quad (2)$$

In an earlier work [5], we found that the approximately separable JPDFs constructed in this manner can be well represented by common analytic distribution functions for cubic lattices over a wide range of defect concentrations. We expand upon that work here, exploring the application of our methods and concentrating on the physical causes of IHB due to coordinated pairings of defects in the inner shells. The $P_2(W_2, c)$ distributions are well characterized by the four-parameter alpha-stable distributions [6] and the $P_1(W_1, c)$ distributions are readily fitted with two-parameter gamma distributions. The concentration dependent fit parameters will be discussed in examples to follow. The approximately separable JPDFs constructed by this method are able to reproduce simulated PAC features very well. In principle the use of this method allows for the direct determination of the splitting parameter V_{zz}, the asymmetry parameter η and the defect concentration c in PAC experiments with significant concentrations of static defects. However, we also seek to understand IHB through the process of parsing the JPDF by contributions from specific shells. That is, we wish to know how heavily a particular configuration of defects influences the IHB seen in a G_2 spectrum.

2 Characteristics of the lattice JPDF in point charge simulations

In the point charge defect model a TD in coordination shell 1 defines the z-axis for all cubic lattices. When considered alone, this point maps to the EFG W_1-W_2 plane at the position $(0, 64)$. The main peak of the JPDF forms about this point. Other contributions to the JPDF come from the accumulation of discrete charge configurations coupling to the TD. Figure 1 shows the discrete EFG points that arise from a single defect in shells 2 through 6 and shell 25 pairing with the TD, each in turn. It is readily apparent that the more distant the coupling shell, the closer the resulting EFG point is to the TD main peak. Each shell produces a finite number of such points which generally increases with shell number. Thus the main peak is reinforced from the myriad sea of distant shells. In the limit of low defect concentration the JPDF would consist of just this main peak populated by such contributions. The solid lines in Fig. 1 show the continuous distribution of points that would arise from an amorphous spherical shell of defects at a given shell distance. These lines truncate in the EFG plane at positions corresponding to the lattice midplane relative to the TD z-axis, or $\theta = 90°$. This natural truncation results in an intrinsically asymmetric distribution. The part of the EFG plane below these truncated lines is only accessible by pairings that arise from chance alignments of defects along particular directions in multiple inner shells. This occurs for distributions with high defect concentrations but the distribution nevertheless remains skewed. The background of the figure shows a contour map of the JPDF for the sc lattice with a defect concentration of $c = 3$ %. It can be readily seen that the contours of the JPDF main peak align with, or are bounded by, the lines derived from the amorphous distribution. However there are numerous irregularities and smaller peaks associated with other inner shell pairings.

The limits on the shape of the JPDF in the EFG plane due to coordinated inner shell defect pairings to the TD are defined exclusively by defects in shell 2. This is apparent in Fig. 1 by noticing the limiting bound imposed by the shell 2 line. Insight is gained into

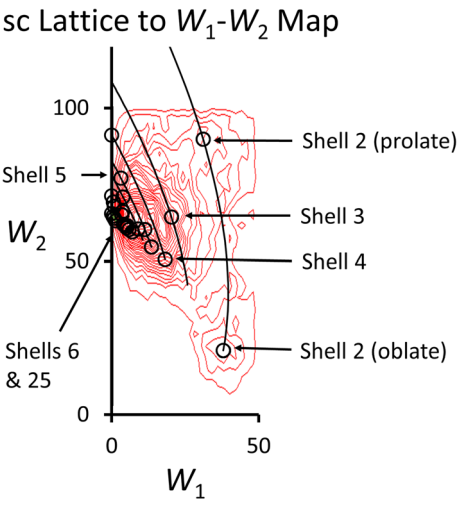

Fig. 1 (Color online) The W_1-W_2 EFG coordinate plane showing the map of discrete lattice pairings between the TD in shell one and lattice sites in shells 2 through 6, and shell 25. Probability density grows about these points when coupled to other charge configurations. The *solid lines* passing through these points represent the result of considering an amorphous distribution of charges in spherical shells, thus highlighting the discrete and spiky nature of the distributions expected from discrete lattices. The background image (*red*) shows the JPDF contour map for the sc lattice and a defect concentration of $c = 3$ %

the development of the JPDF from such discrete points by examining the mapping of a combination of lattice charge defects to the EFG W_1-W_2 plane. Consider the EFG arising solely from the TD, a defect in shell 2 and a defect in one additional shell. We denote this coupling as (TD + shell 2 + 1). This process illustrates the ultimate limiting width and shape of the JPDF. Consider Fig. 2 in which the loci of points generated by this prescription are displayed for the sc lattice. There are two points in the EFG plane from the (TD + shell 2) pairing alone. The points are at the centers of the largest set of circles in the left panel of Fig. 2. The uppermost point can be thought of as coming from a more prolate arrangement, and the lower from a more oblate one. The effect of building a peak of probability density is illustrated by then finding the EFG points corresponding to the combinations of (TD + shell 2 + 1) for many additional shells. The figure displays the results from shells 3 through 11 and shell 25. The points are at the centers of circles whose radii decrease with increasing shell number so that the contributions from shell 2 are the largest circles and those from shell 25 are very small circles. These are nearly indistinguishable in the figure and entirely circumscribed by the circles marking shell 2. The resulting distributions represent peaks of probability density aligned with the shell 2 defects. All other inner shell defects also couple strongly with the TD to form such peaks. The right panel in Fig. 2 shows two examples of this. The peak denoted with squares comes from the (TD + shell 3 + 1) coupling while the triangles denote the case generated when shell 2 has two defects in it, denoted in the figure as (TD + shell 2 × 2 + 1). Note that the width of any peak generated by pairing to the TD is determined by the neighboring shell. For instance, Fig. 2 shows that the points from shell 3 are the most distant from the center of the shell 2 peaks, and conversely, the contributions from more distant shells are progressively closer. More complex pairings, such as that illustrated by the doubly occupied shell 2 example in the right panel of Fig. 2 are those which develop probability density in the extreme regions of the EFG plane, and go well beyond the limits shown for singly occupied shells indicated in Fig. 1. The presence of such peaks in the JPDF are then clearly a function of defect concentration. This process which defines the growth of peaks within the JDPF is identical to the way the main peak itself is constructed. Thus every such minor peak in the JPDF is broadened in the identical fashion to the main peak. We note that the width of the JPDF is not necessarily determined by the width of the main peak alone. The (TD + shell 2 + other) pairings give rise to the

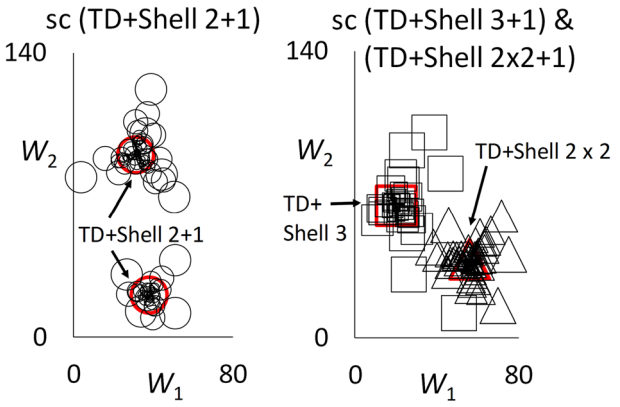

Fig. 2 (Color online) *Left Panel*: a TD in shell 1 is coupled to a point charge in shell 2 (in all possible orientations) for the sc lattice. A third charge couples to these by successively visiting all the lattice sites in shells 3 through 11 and shell 25. Each combination produces a discrete point in the W_1-W_2 plane. The points from each shell are indicated by the size of the circle. The *largest circles* (*red*) are from the (TD + shell 2) pairing alone. The (TD + shell 2 + shell 3) points are the next largest circles and so on. The closer the inner shell pairings, the further the spread of the points in the EFG plane. The accumulation of such points builds a peak of probability density in the JDPF. The spread or width of the JPDF is then determined by such pairings. *Right Panel*: A peak resulting from the (TD + shell 3 + 1) pairing to a defect in shells 2 to 10 (*boxes*) and a peak from the double occupancy of shell 2 (TD + shell $2 \times 2 + 1$) with a defect from shells 3 to 10 (*triangles*)

greatest spread in peak locations and these, when populated, determine the width of the JPDF.

The final form of the JPDF derives from the near countless possible couplings of charge distributions, but the central point of the simulations here is to illustrate that only a few inner shell pairings are important in determining the ultimate physics that derives from the JPDF. The two main features of the distribution are location of the peak and its overall width. Figure 3 illustrates the piecewise construction of the JPDF for the sc lattice for a defect concentration of $c = 5$ %. The defect concentration of 5 % is chosen to insure sufficient probability of finding shell 2 occupied. In the left panel of Fig. 3 only the defects found in shells 2 through 5 are used to accumulate the JPDF. The distribution is best described as "spiky". It is discontinuous and composed of many discrete peaks. The highest peak is the one derived from the pairing of the TD with all remote configurations. The next highest peaks come from the pairing of the (TD + shell 2 + 1) defects or the (TD + shell 3 + 1) defect configurations. Smaller peaks involve the TD and a single defect in some other inner shell pairing and so on. The right panel in Fig. 3 includes contributions from shells 2 through 72. There are now countless minor peaks, but the morphology of the whole is established by the core set of peaks from the inner shells. Notice in particular that there is a substantial minor peak to the right of the main block of probability density that comes from shell 2. Of interest here is how well the G_2 spectrum can be represented by the limited amount of information in shells 2 to 5. This is illustrated here by producing the associated G_2 spectrum from each distribution and comparing them. The middle panel of Fig. 3 compares the simulated G_2 spectrum from each case. The dotted line is for the JDPF from shells 2 to 5 and the solid line is the result from the full distribution. The differences in the two spectra are minor. It can be observed that the information from just shells 2 through 5 would be sufficient to capture the hyperfine frequencies, and it accounts for nearly all of the width or IHB of the spectrum. Apparently the average width of the distribution and average mean

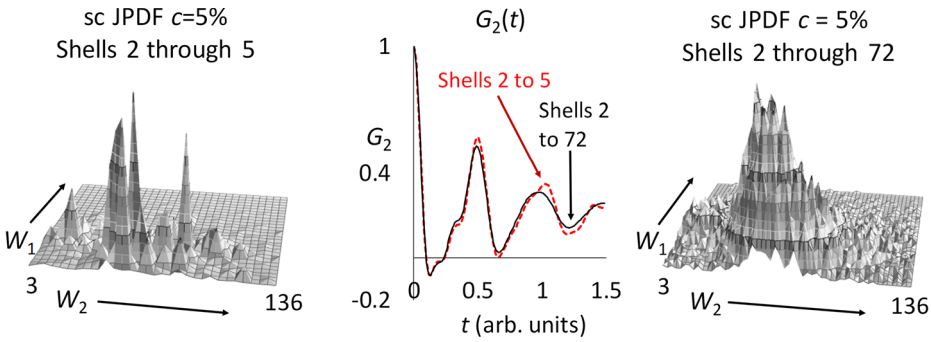

Fig. 3 (Color online) The JPDF for the sc lattice for a defect concentration of $c = 5$ % as constructed from defects confined to shells 2 through 5 (*Left Panel*) and as composed from defects present through shell 72 (*Right Panel*). The middle panel compares the G_2 spectrum derived from each simulation. Although the first simulation carries information from just the first five shells and has an extremely spiky JPDF, the G_2 spectrum it produces (*red dashes*) is virtually the same as that formed from the full JPDF (*black*). Apparently the basic determining factor for the spectrum is the width and peak location of the distribution, and the simulation containing contributions from just shells 2 through 5, though discrete and discontinuous, has the same average peak location and width as the more developed JPDF

as may be defined for the spiky, discrete JPDF is sufficient to convey enough physics to determine the G_2 spectrum. As with other examples shown here, results from the other cubic lattices show the same behavior.

The representation of cubic lattice JPDFs is now complicated by the discrete features described above. The main goal of achieving a set of two approximately independent PDFs with which to characterize the PAC-observables can only be considered by some appropriate means of smoothing and averaging the spiky JPDF. We have chosen to use marginal PDFs as described below to model the JPDF. In this process, some of the details of the overall skewing of the JPDF due to the bounding limits of the lattice mapping, and of the skewing due to discrete isolated peaks from inner shell pairings may be lost. Examples illustrating such limitations are given below.

3 Modeling the JPDF with marginal distributions

The marginal distribution $P_1(W_1, c)$ represented in terms of the gamma distribution with mean μ and variance σ is

$$P_1(W_1) = \frac{W_1^{(\mu^2/\sigma-1)}}{\Gamma(\mu^2/\sigma)(\sigma/\mu)^{\mu^2/\sigma}} \exp(-\mu W_1/\sigma). \tag{3}$$

The alpha-stable distribution used to represent $P_2(W_2, c)$ is found from the integration of

$$P_2(W_2) = \frac{1}{2\pi} \int_{-\infty}^{\infty} \exp(i(\delta - W_2)t - |\gamma t|^{\alpha}(1 - i\beta \mathrm{sgn}(t) \tan(\pi\alpha/2)))dt. \tag{4}$$

The parameters γ and δ represent respectively the width and the peak location for $P_2(W_2)$. The parameter β is the "skewness" parameter. The parameter α is called the "stability parameter" and essentially describes the type of envelope the distribution has. The case

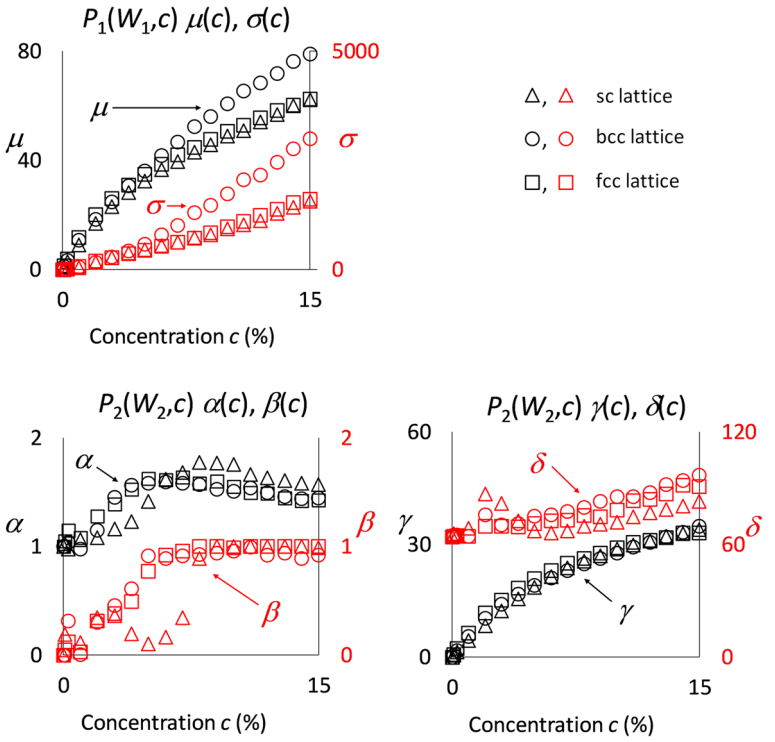

Fig. 4 (Color online) The concentration dependence of the parameters of $P_1(W_1, c)$ and $P_2(W_2, c)$ for cubic lattices. *Circles* are bcc, *triangles* sc, and *squares* fcc. *Top Panel*: $P_1(W_1, c)$ is modeled with a gamma distribution with mean μ (*black*) and variance σ (*red*). The bcc lattice is clearly distinguishable from sc and fcc in μ and σ for moderate defect concentrations. *Bottom Panels*: $P_2(W_2, c)$ is modeled with an alpha-stable distribution, using parameters α (stability, in *black*), β (skewness, in *red*), γ (peak width, in *black*) and δ (peak location, in *red*). The γ parameter is most sensitive to c, and δ generally increases with c. The parameters α and β show complex behavior at low c, but otherwise tend to saturate at higher concentrations

$\alpha = 1$ corresponds to a Lorentzian distribution while for $\alpha = 2$ ($\beta = 0$), the distribution is Gaussian. The fitting parameters for each distribution are strongly concentration dependent.

Figure 4 shows the fit parameters for the marginal distributions $P_1(W_1, c)$ and $P_2(W_2, c)$ for the three cubic lattices. The mean μ and the variance σ for the $P_1(W_1, c)$ gamma distribution fits are shown in the top panel. They increase smoothly with c. The differing symmetry of the bcc lattice is most clearly reflected in σ and μ for which the bcc values of each increase faster with concentration than in sc or fcc. This can be accounted for by comparing the relative lattice distances between shell 2, the TD in shell 1 and the probe. For the sc and fcc lattices the ratio of the distance from shell 2 to the TD to the probe is $\sqrt{2}$:1:1, while for bcc it is $\frac{2}{\sqrt{3}}$:1:1. The relative effects on the EFG tensor of pairings between inner shell defects and shell 2 depend on the inverse cube of this ratio and are therefore stronger in the bcc lattice. The spreading of the JPDF in the W_1-W_2 plane at larger concentrations is dominated by instances of multiple occupancy of defects in shell 2 pairing with other nearby charge configurations. In fact, pairings from multiply occupied shells tend to move the distribution mean outward along the W_1 axis more strongly than along the W_2 axis, shifting the mean of the P_1 distribution more than occurs for the P_2 distribution. That the

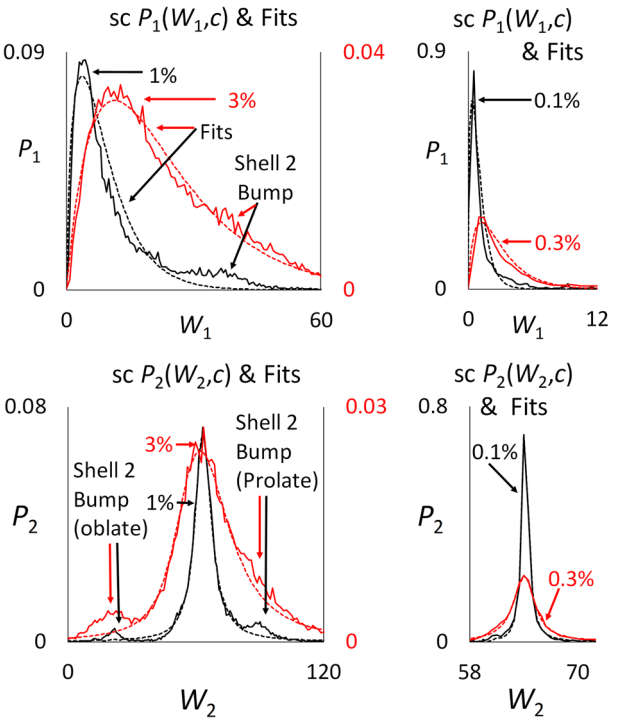

Fig. 5 (Color online) The marginal PDFs $P_1(W_1, c)$ (*top panels*) and $P_2(W_2, c)$ (*bottom panels*) for the sc lattice in the point charge model. *Solid lines* are from PAC simulations, *dashed lines* are fits to the PDF. Defect concentrations are shown on the right for $c = 0.1$ % (*black*) and 0.3 % (*red*) and for 1 % (*black*) and 3 % (*red*) in the left panels. *Top Left*: Gamma distribution fits to $P_1(W_1, c)$. For $c = 1$ % shell 2 is populated enough to produce a strong bump in the distribution. By $c = 3$ % the bump is less noticeable. The effect of the bump on the fit is to pull the fit to the right, increasing the mean and width of the fit. *Top Right*: At low concentrations shell 2 is rarely occupied and the PDF is very narrow. P_1 is determined by the TD and the effects from distant diffuse charges. *Bottom Right*: Low concentration, $c = 0.1$ % and 0.3 % alpha stable fits to P_2. With little contribution from shell 2, the PDFs are very narrow, nearly Lorentzian and centered at $W_2 = 64$. *Bottom Left Panel*:P_2 and its fit at moderate concentrations $c = 1$ % and 3 %. Shell 2 produces strong bumps near $W_2 = 20$ and $W_2 = 90$. The rightmost peak in the $c = 3$ % case is less pronounced because other peaks grew and spread. However the peak on the left is more pronounced. The peak at $W_2 = 20$ is farther from the ($W_2 = 64$, $W_1 = 0$) TD origin and thus its inner shell pairings remain distinct at higher concentrations. This region of EFG space is populated by contributions from inner shell combinations in the mid-plane of the lattice. At higher concentrations both bumps blend smoothly in the the JPDF

bcc lattice has an intrinsically larger coupling factor accounts for the observed pattern. The P_1 parameters otherwise vary smoothly with concentration reflecting the steady increase of inner shell pairings.

The lower panels in Fig. 4 show the fit parameters for $P_2(W_2, c)$ using the alpha-stable distribution. The complex behavior seen in the parameters for $P_2(W_2, c)$ strongly reflects the changes in the JPDF where inner shell pairings are most pronounced. Considering each parameter in turn, γ, which reflects the width of P_2 shows virtually the same concentration dependence for each lattice. It increases smoothly from zero but appears to saturate with concentration. The peak location δ is a generally increasing function of concentration with the exception of the low concentration dependence in the sc lattice. A similar irregularity

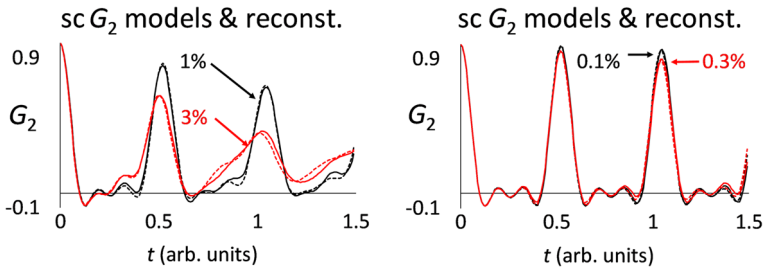

Fig. 6 (Color online) The PAC spectra $G_2(t, c)$ for the sc lattice for point charge defect concentrations $c = 1$ % (*black*), 3 % (*red*), in the left panel and 0.1 %, (*black*) and 0.3 % (*red*) in the right panel. The *solid lines* are from PAC simulations and the *dashed lines* are reconstructions using the marginal PDFs. Despite the spiky nature of the actual JDPFs the marginal PDFs produce spectra that would be precise enough for experimental discrimination of defect concentration. The distortions to the marginal PDFs from shell 2 are most pronounced for $c = 1$ % and to a lesser extent in the case for 3 %. Both cases are still fitted reasonably well

for the sc parameters α and β are evident. For this case, the more open structure of the sc lattice may contribute heavily to this irregularity. At low concentrations there is little chance of finding a defect in shell 2. The skewing of the JDPF is then determined by some other inner shell with the highest probability of being occupied. It is not immediately obvious how this affects the complex determination of the α-stable fit parameters. We note only that when the concentration of defects is high enough to insure occupancy of shell 2, that the sc parameters then fall much more in line with the behavior of the other two lattices. The increase in δ with concentration also reflects the addition of many more coordinated sets of aligned defects and multiply occupied shells that can spread the JPDF away from the TD-induced main peak. Interestingly the β parameter saturates quickly with concentration. At low defect concentrations, the symmetry of the JPDF is dominated by the TD-induced main peak and while it is not wholly symmetric it integrates into a marginal distribution for P_2 that is nearly Lorentzian. Thus β is nearly zero for low concentrations. As the inner shells become more populated the lattice-imposed limits on the EFG plane favor distributions that are skewed to higher values of W_2, and β thus increases. At sufficiently high concentrations, where shell 2 is clearly occupied, the skewing saturates. In a similar fashion the stability parameter α starts at low concentration with a value near 1, giving a Lorentz-like shape of the distribution envelope and tail. At high concentrations the blended peaks in the JPDF become thicker near the mean relative to the tail, and α increases. The limiting value appears to be near 1.5. We note that the Gaussian distribution is characterized by $\alpha = 2$.

For purposes of illustration the fitted marginal distributions $P_1(W_1)$ and $P_2(W_2)$ for the sc lattice are shown in Fig. 5 for defect concentrations $c = 0.1$ %, 0.3 %, 1 %, and 3 %. Fits for the fcc and bcc lattices are similar. For defect concentrations $c = 0.1$ % and 0.3 %, seen in the rightmost panels of the figure, occupancy of shells 2 and 3 is negligible, and the PDFs are determined by the TD couplings to remote defects. The resulting peaks are narrow with P_2 being nearly symmetric about $W_2 = 64$. For $c = 1$ % the occupancy in shell 2 has increased. This is immediately apparent in the PDFs. The leftmost panels in Fig. 5 now show a distinct bump in $P_1(W_1)$ to the right of its main peak and two bumps in $P_2(W_2)$, one to the left and one to the right of its main peak. These correspond exactly to the description of the peaks built in Fig. 2. The smooth alpha-stable fits for P_2 do not render these bumps well, so that any resulting PAC quantity calculated from such fits will necessarily

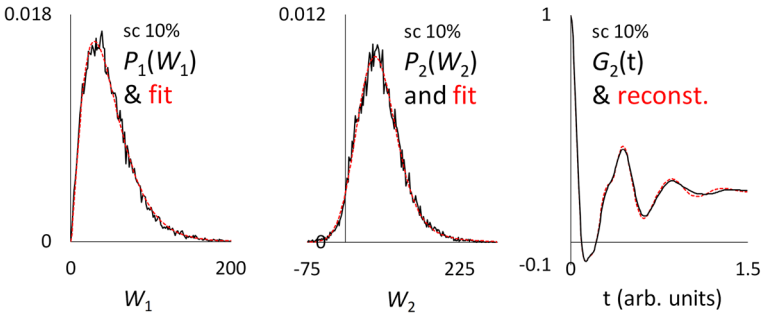

Fig. 7 (Color online) The marginal PDFs $P_1(W_1)$ and $P_2(W_2)$ (*black*) and their fits (*red dashes*) are shown for the sc lattice with $c = 10$ % defect concentration. The simulated experimental PAC spectrum $G_2(t, c)$ (*black*) and its reconstructed fit (*red*) are shown in the right panel. The high quality of the fits makes it difficult to resolve their lines in the figures. At this concentration, the bumps due to shell 2 defects are no longer distinct. The PDFs are fitted well, and the resulting reconstructed fit to the G_2 spectrum is excellent

lose some information from shell 2 contributions. At larger concentrations ($c \approx 10$ %—see Fig. 7) the contributions from shell 2 become more nearly blended into the whole, but at $c = 3$ % only the rightmost peak has blended. The peak near $W_2 = 20$ comes from charge configurations occurring in the lattice midplane, and the configurations that eventually blend with this peak do not occur until the defect concentrations are high. It is more probable for prolate configurations of charges to arise, reflecting the axial bias of the TD. The bump from shell 2 in P_1 seen in the top left panel for the $c = 1$ % case has an interesting effect on the fitting of the PDF. The fit is pulled to the right, increasing the width and mean of the peak and thus for low concentrations the contribution to the calculation of PAC quantities from shell 2 comes from the stretching of the fit. At larger concentrations, this bump in P_1 blends into the PDF as can be seen for the $c = 3$ % case. The bump is there, but less pronounced.

4 Modeling PAC observables

With the parameters for the marginal distributions determined, (3) and (4) can be used to reproduce the PAC $G_2(t, c)$ spectrum and other observables. The four sets of PDFs illustrated for $c = 0.1$ %, 0.3 %, 1 %, and 3 % in the sc lattice in Fig. 5 have been used to reconstruct $G_2(t, c)$ for these concentrations and are displayed in Fig. 6. The case for $c = 10$ % in the sc lattice is added in Fig. 7 to illustrate the effect of higher defect concentrations. The solid lines for G_2 in both figures are the simulated PAC experiments and the dotted lines show the reconstructions from (3) and (4). We note that the fits in all cases are good enough to allow for experimental determination of spectra with IHB on the basis of defect concentration. The fits at both the low and high concentrations are quite good. The fits for the 1 % and 3 % cases show the most deviation from the simulated experiment. This is in line with expectations that the PDFs have the most distortion due to discrete bumps from shell 2 and the subsequent loss of information about the contributions of shell 2 in the fitted PDFs. In all cases, however, the central peaks (and hyperfine frequencies) are well resolved. In Fig. 7 the marginal PDFs for P_1 and P_2 and their fitted distributions are shown for the defect concentration of 10 % along with G_2. In this case the bump evident from shell 2 has been completely lost in the manifold combinations of charge configurations now

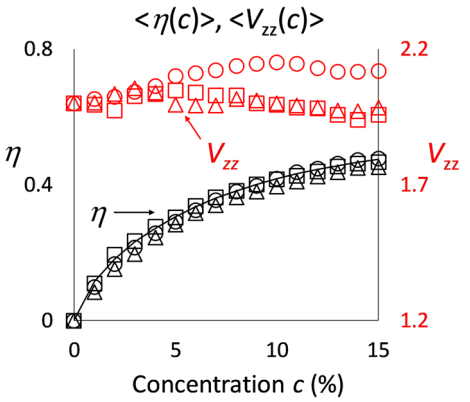

Fig. 8 (Color online) The concentration dependence of the splitting parameter V_{zz} (*red*) and the asymmetry parameter η (*black*) are shown as functions of defect concentration c for the cubic lattices. The sc lattice is marked with triangles, the fcc lattice with squares and the bcc lattice with circles. The parameters are calculated as expectation values from the JPDFs derived from point charge models. Values of V_{zz} in our units vary around 2, with the bcc lattice exhibiting significantly different behavior for high concentrations than that of the fcc and sc cases. A trend line fitted to a hyperbolic tangent has been added to the η-graph

contributing to the JPDF. The reconstructed G_2 is a particularly good fit to the simulated experiment. Cases for the fcc and bcc lattices are similarly well fitted.

With the PDFs determined, other PAC parameters can also be explored. The most relevant experimental parameters are η and V_{zz}. We note that experimental investigations including IHB have traditionally lacked a means to systematically estimate η, and the fit to V_{zz} has often been determined empirically by assuming a Lorentzian or Gaussian distribution [7]. For situations dominated by static point charge distributions, such as investigated here, the determination of η can be directly found from knowledge of the JPDF. Figure 8 shows the determination of the defect concentration dependence of $\eta(c)$ and $V_{zz}(c)$ for our simulation model in all three cubic lattices. It is clear from the figure that η is the more robust parameter for evaluating the effects of defect concentration. For the concentration range explored here, η varies smoothly with concentration varying almost as the square root of c. An approximate fit to the concentration dependence using the hyperbolic tangent function has been added to the figure as an illustration of the simplicity of the η dependence on c. The behavior of V_{zz} is more complex, but it is interesting to note the distinctly different behavior of the bcc lattice in which the average V_{zz} value is higher than for the sc and fcc cases. We again attribute this behavior to the relatively stronger contribution to the JPDF from bcc shell 2 lattice spacing.

5 Discussion

When considered by themselves, the small numbers of lattice sites in the inner coordination shells of cubic materials lead immediately to the skewing of possible JPDFs of EFG components that can be used to characterize PAC phenomena. Defects situated in these inner shells pair up primarily with a TD in shell 1 to produce a limited number of fixed points in any given EFG coordinate plane. Probability density then develops around these points as the limited inner configurations couple to the nearly amorphous contributions from remote

defects. In considering its relation to the main JPDF peak in the EFG coordinate plane, the closer a given defect is to the TD, the more separated its EFG coordinates will be from the main peak. This is the same as saying that the charged defect will contribute more strongly to the combined determination of V_{zz} and η because of the inverse cube dependence of the EFG on distance. For low concentrations from 1 % to 3 % this leads to marginal distributions that have multiple discrete peaks. For larger concentrations these distinct peaks blend well enough to produce approximate single-peaked marginal distributions. Conversely, the further the charge is from the TD, the closer to the central peak its EFG contribution will be.

Interestingly the physics necessary to capture the essential PAC behavior of cubic lattice systems in the point charge model depends almost entirely on the ragged and spiky contributions to the JPDF from the (TD + inner shell) pairings This was shown in Fig. 3 in which the G_2 spectrum found by using only the innermost 5 shells is nearly the same as that found using 72 shells for the particular case illustrated. This result comes from precisely how the JPDF is constructed. The main peak of the JPDF is composed as the limiting sum of contributions of discrete charges in remote shells coupling to the TD. This is the usual explanation of cause of IHB [8]. But the width of the JPDF itself is determined by the distribution of secondary peaks from the coordinated couplings between the TD and inner shell defects acting together which then couple with all remaining remote charge configurations. In effect, with one TD in shell 1, defects in shell 2 essentially define a limiting width and peak location of the JPDF. For the JPDF to have density in regions of the W_1-W_2 plane beyond the bounds set by this (TD + shell 2) coupling requires the alignment of multiple defects in several inner shells. Whether shell two is occupied or not is a function of the defect concentration. For sufficiently low concentrations this is not likely and the width of the JPDF is determined by the diffuse, amorphous-like halo of remote lattice configurations. The ensemble averaging of a PAC-observable against the JPDF is a process of integration and as such the location of the peak and the width of the JPDF are the primary determining factors. The exact nature of the JPDF need not be known with particularly high precision to obtain reasonable physical results as was demonstrated in Fig. 3 for which in the first case the JPDF appears as a ragged assortment of spikes while in the second the JPDF could be characterized with smooth analytic marginal distributions.

The strong coupling between the nearest inner shells creates a strong dependence on concentration for the JPDF. For instance when the occupancy of shell 2 is negligible, as it is for low concentrations, $P_2(W_2, c)$ is nearly Lorentzian. The IHB that arises in this case comes only from the TD coupling to the halo of amorphous-like remote charge configurations. As the occupancy of the inner shells increases, these pairings skew the JPDF and widen its envelope relative to the distribution tail. As noted in the discussion of Fig. 4 this increases α in the fits to $P_2(W_2, c)$ from 1 to about 1.5. For a transitional range of c, the marginal distributions cannot be readily fitted by a single distribution function, but even in these cases, having an approximate peak location and distribution width allows for reasonable determination of PAC parameters.

The predicted concentration-dependent values for η and V_{zz} in Fig. 8 are found as expectation values by integration against a JPDF which intrinsically contains information about the asymmetries of the EFG tensor. On the other hand, experimental values of η are typically derived from fits to an expression that is an integration against an assumed PDF of V_{zz} values alone [7, 9–11],

$$G_2(\eta, V_{zz}^o, t) = \int dV_{zz} G_2(\eta, V_{zz}, t) P(V_{zz} - V_{zz}^o) \tag{5}$$

where V_{zz}^o is the peak value of V_{zz} in $P(V_{zz} - V_{zz}^o)$ that is usually assumed to be either Gaussian or Lorentzian or a mixture of the two. Fits to the resulting form

$$G_2(\eta, V_{zz}^o, t) = S_{20}(\eta) + \sum_n S_{2n}(\eta) \cos(\omega_n(\eta, V_{zz}^o)t) \exp\left[-\frac{1}{p}(\delta\omega_n(\eta, V_{zz}^o)t)^p\right] \quad (6)$$

give η, V_{zz}^o and δ. The latter parameter is simply related to the FWHM of the distribution. The value $p = 2$ is for a Gaussian distribution and $p = 1$ for Lorentzian. Interestingly, examination of distributions of V_{zz} in our simulations shows that these clearly evolve from Lorentzian toward Gaussian with increasing defect concentration. This effect should be discernible in experimental PAC spectra showing IHB. Experimenters have also used intermediate values of p in their analyses. For instance Collins and Sinha [10] used $p = 1.25$ while Nieuwenhuis et al. [11] used $p = 3/2$. The connection between p and defect concentration in experiments remains to be explored. We have verified that the expectation values in Fig. 8 self-consistently match those obtained by fits to (6). For instance, arbitrarily examining the simulation for fcc, $c = 5$ %, with $p = 2$, the values obtained for η and V_{zz} from (6) differ from those of Fig. 8 by less than 1 %, η(JPDF) $= 0.3035$ versus η (6) $= 0.3025$ and V_{zz}(JPDF) $= 2.045$ versus V_{zz} (6) $= 2.065$. The results presented in Fig. 8 apply only to situations in which a point charge model in the specific cubic symmetries presented here are applicable. Application to other symmetries and charge models requires determining the appropriate JPDFs from suitable models.

6 Conclusions

We have used the W_1-W_2 parameterization of the EFG tensor to examine IHB in cubic symmetries and have described suitable JPDFs that accurately reproduce IHB in PAC spectra. We have demonstrated the physical cause of IHB in PAC spectra as it arises from individual contributions from coordinated pairings of defects near probe nuclei and its TD partner and shown how this gives rise to a complex, spiky structure for the JPDF. We have determined the defect concentration dependence of PAC spectra subject to IHB over a broad range of concentrations. In all cases we examined, the skewed JPDF can be reduced to marginal distributions, $P_1(W_1, c)$ and $P_2(W_2, c)$ that reproduce PAC observables very well. We have also demonstrated that the basic physics necessary to model PAC spectra comes from the discrete and ragged assortment of peaks generated from inner shell pairings, which allows us to conclude that precise knowledge of the JPDF is not necessary as long as the width and peak location of the JPDF can be reasonably characterized. In particular, we have described how the coupling between the TD and shell 2 accounts for the evolution of the JDPF with defect concentration. We have shown that PAC-relevant parameters such as η and V_{zz} can be calculated from the PDFs described here and that these calculated values are consistent with those derived from empirical fits to G_2 spectra.

While we have explicitly used a point charge model in our simulations, more sophisticated methods such as density functional models could be applied but the basic conclusions about IHB in cubic symmetries should remain. That is the effects of IHB are strongly influenced by particular configurations of defects in the inner shells. It is not sufficient to consider broadening only from average remote distributions of charges. The JPDF is fundamentally widened and distorted by these inner shell contributions, and results in more pronounced broadening than from remote defects only. The methods we have used to characterize the JPDF of cubic structures should find ready application to a variety of similar hyperfine phenomena.

References

1. Czjzek, G.: Distribution of nuclear quadrupole splittings in amorphous materials and the topology of the (V_{zz}, η)-parameter Space. Hyperfine Interact. **14**, 189–194 (1983)
2. Evenson, W.E., Adams, M., Bunker, A., Hodges, J.A., Matheson, P.L., Park, T., Stufflebeam, M., Sullivan, F.P., Zacate, M.O.: Topologically Appropriate Coordinates for (V_{zz}, η) Joint Probability Distributions. Hyperfine Interact. **237**, 119 (2016)
3. Czjzek, G., Fink, J., Goetz, F., Schmidt, H., Coey, J.M.D., Rebouillat, J.-P., Lienard, A.: Atomic coordination and the distribution of electric field gradients in amorphous solids. Phys. Rev. B **23**, 2513 (1981)
4. Stöckmann, H.-J.: Electric field gradients resulting from randomly distributed unscreened point charges. J. Mag. Res. **44**, 145–158 (1981)
5. Evenson, W.E., Adams, M., Bunker, A., Hodges, J., Matheson, P., Park, T., Stufflebeam, M., Zacate, M.O.: Inhomogeneous broadening of PAC spectra with V_{zz} and η joint probability distribution functions. Hyperfine Interact. **222**, 77–86 (2013)
6. Nolan, J.P.: Levy Processes, pp. 379–400. Birkhäuser, Boston (2001)
7. Zacate, M., Jaeger, H.: Perturbed angular correlation spectroscopy—a tool for the study of defects and diffusion at the atomic scale, defect and diffusion forum. ISSN: 1662-9507, **311** 3–38 (2011)
8. Stoneham, A.M.: Shapes of inhomogeneously broadened resonance lines in solids. Rev. Mod. Phys. **41**, 82–108 (1969)
9. Forker, M.: The problematic of the derivation of the electric field gradient asymmetry parameter from TDPAC measurements or Mössbauer spectroscopy in imperfect crystal lattices. Nucl. Instrum. Methods **106**, 121–126 (1973)
10. Collins, G.S., Sinha, P.: Structural, thermal and deformation-induced point defects in PdIn. Hyperfine Interact. **130**, 151–179 (2000)
11. Nieuwenhuis, E.R., Collins, G.S., Favrot, A., Zacate, M.O.: High-temperature polymorph of In_2La. J. Alloys Compd. **387**, 20–23 (2005)